



The seasonal footprinting mechanism in large ensemble simulations of the second generation Canadian earth system model: uncertainty due to internal climate variability

Shangfeng Chen¹ · Bin Yu²

Received: 23 October 2019 / Accepted: 24 July 2020 / Published online: 30 July 2020
© The Author(s) 2020

Abstract

Previous studies indicated that the wintertime North Pacific Oscillation (NPO) could exert marked impacts on the following winter El Niño–Southern Oscillation (ENSO) via the seasonal footprinting mechanism (SFM). Here, we examine this winter NPO–ENSO relationship in a 50-member ensemble of historical simulations conducted with the Canadian Centre for Climate Modeling and Analysis second generation Canadian Earth System Model (CanESM2) over the period of 1950–2005. The observed NPO pattern, featured by a meridional dipole atmospheric anomaly over the North Pacific, can be well reproduced by all of the 50 ensemble members. The multi-member ensemble (MME) mean can well simulate the observed NPO–ENSO relationship, as well as the SFM process. However, there exists a large spread of the results among the 50 members due to internal climate variability. Internal climate variability influences the winter NPO–ENSO relationship through modulating the subtropical center of the NPO. Specifically, the ensemble members with high NPO–ENSO correlations tend to have strong atmospheric anomalies over the subtropical North Pacific in winter. The atmospheric circulation anomaly brings strong sea surface temperature and precipitation anomalies in the tropical central Pacific and westerly wind anomalies over the tropical western Pacific in the following spring. These anomalies sustain in the following seasons and eventually lead to ENSO events in the following winter.

Keywords NPO · ENSO · Seasonal footprinting mechanism · Large ensemble simulations · Internal climate variability

1 Introduction

The El Niño–Southern Oscillation (ENSO) is the leading air–sea coupled mode over the tropical Pacific on the inter-annual timescale (Bjerknes 1969; Philander 1990; Neelin et al. 1998; Wang et al. 2000; Alexander et al. 2002). ENSO events have substantial influences on ecosystems, marine, crop growth, extreme weather and climate events over many regions surrounding the Pacific and remote areas through oceanic and atmospheric teleconnections (Luo et al. 2011; Chiang and Sobel 2002; Huang et al. 2004; McPhaden,

2002; Wu et al. 2003; Song et al. 2017; Zhang et al. 2017, 2019a; Chen et al. 2018a, b, c, d; Jin et al. 2018; Chen and Song 2019; Wang et al. 2019; Chen et al. 2019; and references therein). For example, ENSO can significantly affect East Asian climate via altering the atmospheric circulation anomalies over the subtropical western North Pacific (Wang et al. 2000; Xie et al. 2009; Zhang et al. 2019b). In an El Niño winter, a significant anticyclonic anomaly can be induced over the subtropical western North Pacific. The associated southerly wind anomalies along the east coast of East Asia would reduce intensity of the East Asian winter monsoon, leading to above normal surface temperatures over many parts of East Asia (e.g. Wang et al. 2000; Zhang et al. 2019b). Meanwhile, the winter El Niño-generated anomalous anticyclone over the subtropical western North Pacific could maintain into the following summer via the local positive air–sea feedback process (Wang et al. 2000), as well as modulating the sea surface temperature (SST) anomalies in the Indian Ocean (Xie et al. 2009) and North Atlantic Ocean (Rong et al. 2010; Chen et al. 2018a, b, c, d; Zhao

✉ Shangfeng Chen
chenshangfeng@mail.iap.ac.cn

¹ Center for Monsoon System Research, Institute of Atmospheric Physics, Chinese Academy of Sciences, Beijing, China

² Climate Research Division, Environment and Climate Change Canada, Toronto, ON, Canada

et al. 2019), which further exert impacts on the following East Asian summer climate. In addition, ENSO influences the North American climate via inducing a Pacific-North American atmospheric teleconnection pattern (Wallace and Gutzler 1981; Yu and Zwiers 2007), the south Pacific and south American climate via triggering a Pacific-south American atmospheric teleconnection (Mo 2000), and the Eurasian climate via the stratospheric process (Graf and Zanchettin 2012). Furthermore, tropical cyclone activities over Atlantic, Pacific and Indian Oceans are also significantly modulated by ENSO events (Gray 1984; Chan 2005). Given these marked ENSO impacts on weather and climate systems over the globe, it is of great importance to investigate the ENSO variability and its associated formation and maintenance mechanisms.

It is well recognized that the air-sea interaction and oceanic dynamic processes are dominant factors for the ENSO variability (Bjerknes 1969; Jin 1997; Schopf and Suarez 1988). In particular, initial SST perturbations can develop into an ENSO event via the Bjerknes positive air-sea feedback process (Bjerknes 1969). The tropical Pacific oceanic waves (including westward propagating Rossby waves and the equatorial eastward propagating Kelvin wave) play a crucial role in the transition of ENSO cycle phases (Schopf and Suarez 1988; Jin 1997). In addition, more and more studies showed that the extratropical atmosphere-ocean forcing also plays important roles in modulating the occurrence and amplitude of ENSO events (e.g. Vimont et al. 2001, 2003a; Nakamura et al. 2006; Alexander et al. 2010; Chen et al. 2014, 2017, 2018a; Zhang et al. 2018; Luo et al. 2018).

Regarding the extratropical atmospheric forcing on ENSO, studies indicated that the North Pacific Oscillation (NPO) during the boreal winter could exert a significant impact on the following winter ENSO outbreak via the seasonal footprinting mechanism (SFM; Vimont et al. 2001, 2003a). The NPO is usually defined as the second empirical orthogonal function (EOF) mode of atmospheric circulation variability over the extratropical North Pacific (e.g. Yu and Kim 2011; Park et al. 2013; Chen and Wu 2018), which is characterized by a meridional dipole circulation anomaly pattern over the North Pacific (Fig. 1) (Wallace and Gutzler 1981; Linkin and Nigam 2008; Park et al. 2013; Song et al. 2017; Chen and Wu 2018). Vimont et al. (2003b) further examined the winter NPO-ENSO relationship in a coupled generation circulation model from the Commonwealth Scientific and Industrial Research Organization (CSIRO). They found that the CSIRO model could reasonably well capture the SFM process related to the NPO. The winter NPO accounts for approximately 20–40% of the interannual ENSO variability. Broadly similar results have also been reported from other coupled air-sea generation circulation models (Alexander et al. 2010; Pegion and Alexander 2013). A recent study reported that only a few CMIP5 models can

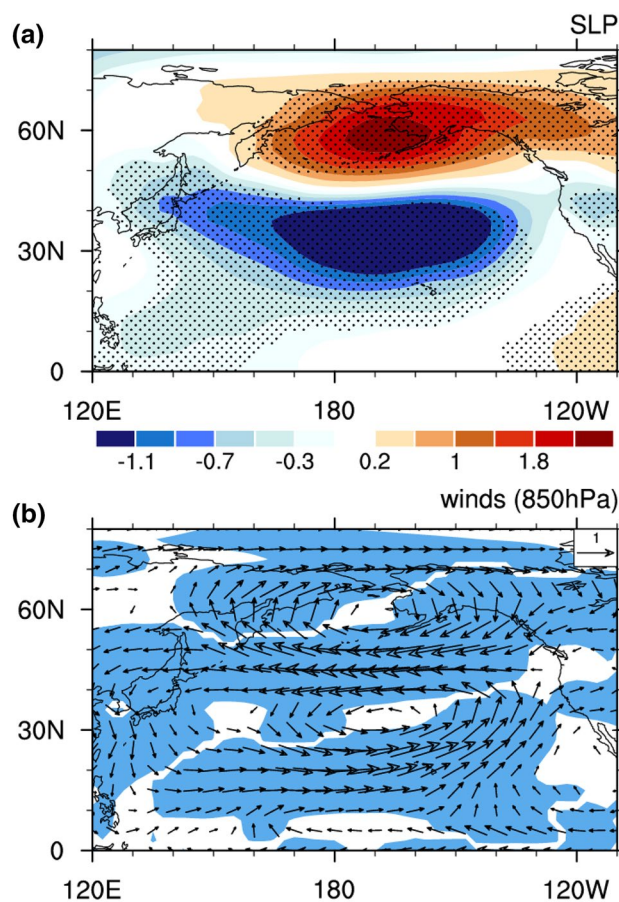


Fig. 1 Regression of ND(-1)JFM(0) SLP (a, unit: hPa) and 850-hPa wind (b, unit: m s^{-1}) anomalies onto the normalized ND(-1)JFM(0) NPO index during 1951–2004 based on the observational data. Stippling region in **a** indicates SLP anomalies significant at the 5% level. Shading region in **b** indicates either direction of the wind anomalies significant at the 5% level. Wind anomalies at both directions less than 0.2 m s^{-1} are omitted

capture the winter NPO-following winter ENSO relation and the associated SFM (Wang et al. 2019).

Recently, large ensemble simulations from coupled climate models have been used to explore climate variability and detect future climate change projections (Deser et al. 2012a, b, 2014; Sigmond and Fyfe 2016; Kirchmeier-Young et al. 2017; Dai and Bloecker 2019; Chen et al. 2019). The role of internal climate variability on current climate anomalies and projected climate changes has been highlighted. It is unclear whether the observed impact of the winter NPO on the following winter ENSO via the SFM process can be reproduced in these large ensemble simulations and whether internal variability plays a role on this NPO-ENSO relationship. In the present study, we will examine the seasonal footprinting mechanism related to the winter NPO in a 50-member ensemble of historical simulations conducted with the Canadian Centre for Climate Modeling and Analysis (CCCma) second-generation Canadian Earth System

Model (CanESM2; Kirchmeier-Young et al. 2017; Sigmond and Fyfe 2016). Each of the CanESM2 ensemble members is forced by a same external forcing but with slight differences in the initial condition, as detailed below in the next section. Hence, the spread in the NPO-ENSO connection among these 50 ensemble members is solely due to the internal climate variability (e.g. Deser et al. 2012a, b). Understanding the influence of internal climate variability on the winter NPO-ENSO relationship and associated physical processes has important implications for the climate model validation and improvement, and for future projected changes of the ENSO variability.

The structure of this manuscript is as follows. Section 2 describes the data and method employed in this analysis. Section 3 examines the winter NPO-ENSO relation in the observation and in the CanESM2 large ensemble simulations. Section 4 investigates the spread of NPO-ENSO connections among the 50 ensemble members and discusses the role of internal climate variability. Section 5 provides a summary and discussion.

2 Data and methods

The present study uses the monthly mean sea level pressure (SLP), horizontal winds, surface heat fluxes (including surface latent and sensible heat fluxes, and surface shortwave and longwave radiations) and precipitation from the National Centers for Environmental Prediction-National Center for Atmospheric Research (NCEP-NCAR) reanalysis (Kalnay et al. 1996; <ftp://ftp.cdc.noaa.gov/Datasets/ncep.reanalysis.derived/>). The NCEP-NCAR reanalysis data is available since January 1948. SLP and horizontal winds from the NCEP-NCAR reanalysis have a horizontal resolution of $2.5^\circ \times 2.5^\circ$, while precipitation is on T62 Gaussian grids. Values of the surface heat fluxes are taken to be positive (negative) when their directions are downward (upward), which contribute to surface warming (cooling). The monthly mean SST data is obtained from the National Oceanic and Atmospheric Administration (NOAA) Extended Reconstructed SST version 3b (ERSSTv3b) dataset (Smith et al. 2008) for the period of 1854 to 2019 (<https://www.esrl.noaa.gov/psd/data/gridded/>). This SST dataset is on a $2.0^\circ \times 2.0^\circ$ longitude-latitude grid. For convenience, the NCEP-NCAR reanalysis data and ERSSTv3b SST are considered as “observational” data in the following analysis.

This study also employs the large ensemble climate simulations of 50 members (Sigmond and Fyfe 2016; Kirchmeier-Young et al. 2017) from the CanESM2, which is a fully coupled ocean-atmosphere-land-sea ice general circulation model (Christian et al. 2010; Arora et al. 2011). Specifically, five simulations are firstly performed

for the period of 1850–1950 to produce five different oceanic states in 1950. Ten experiments are then run from each of the above five historical simulations with slightly different initial conditions in 1950, generating 150-year simulations for the period of 1950–2100 and resulting in a total of 50 ensemble members. Each of the simulations is forced with historical greenhouse gas concentration, sulfate aerosols, and other radiative forcings from 1950 to 2005. From 2006 to 2100, the simulations are forced by the representative concentration pathway 8.5 (RCP8.5, Vuuren et al. 2011). Due to chaotic natures of the climate system, the slightly different initial condition in 1950 can quickly lead to different atmospheric states a few days later (Deser et al. 2012a; Wallace et al. 2014; Kay et al. 2015). The CanESM2 simulations have a horizontal resolution of about $2.8^\circ \times 2.8^\circ$ in longitude-latitude grids.

In this study, the CanESM2 historical simulations over 1950–2005 are analyzed and compared against the observational data. All the variables from the CanESM2 simulations and from observations are interpolated to a common horizontal resolution of $2.5^\circ \times 2.5^\circ$ to facilitate comparisons and calculate spatial correlations. The multi-member ensemble (MME) mean is defined as the equally weighted average of involved members. In addition, as this study concentrates on the interannual relationship between the winter NPO and following winter ENSO, all variables analyzed are subjected to a 2–9-year Lanczos bandpass filter to extract their interannual variations (Duchon 1979). Significance levels of correlation coefficients and anomalies obtained from regression analyses in the observation and each of the 50 members are estimated according to a two-tailed Student’s *t* test. Following previous studies (Deser et al. 2012b; Kucharski and Joshi 2017; Zheng et al. 2018; Joshi and Ha 2019), MME anomalies obtained from regression analyses are statistically significant at the 95% confidence level when it satisfies the following criterion:

$$|MME_var| \geq \frac{std_var \times \lambda}{\sqrt{N}}$$

where $|MME_var|$ represents the absolute value of the MME anomalies; std_var denotes the standard deviation of the anomalies among the members; N is the number of members employed to calculate the MME; and λ is equal to 1.96.

Following previous studies (Battisti 1988; Vimont et al. 2003a; Chen et al. 2014), the present analysis employs the equatorial oceanic Kelvin wave forcing function (KWF) to describe the dynamic response of tropical ocean to the perturbation in surface wind stress anomalies. The equatorial oceanic KWF is expressed as follows (Vimont et al. 2003a; Chen et al. 2014):

$$K_f(x, \lambda) = \int_{30^{\circ}\text{S}}^{30^{\circ}\text{N}} \tau_x(x, y, \lambda) \psi_o(y) dy$$

where x (y) represents longitude (latitude). $\tau_x(x, y, \lambda)$ denotes surface zonal wind stress anomalies at a specific time λ . $\psi_o(y)$ is the meridional structure of the equatorial Kelvin wave. Meridional structure of the equatorial Kelvin wave can be derived through solving the dynamic equation of ocean in the upper-layer under the equatorial β plane (Gill 1980; Vimont et al. 2003a). Amplitudes of the equatorial Kelvin waves weaken exponentially away from the equator. Positive values of KWF indicate that surface wind stress anomalies induce eastward propagating and upwelling Kelvin waves that lead to SST warming (Battisti 1988; Vimont et al. 2003a; Chen et al. 2014).

3 NPO-ENSO relationship in observation and CanESM2

We first examine the connection of the winter (November–December–January–February–March-average, ND(−1) JFM(0) for short) NPO with ENSO in the subsequent winter (December–January–February-average, D(0)JF(+1) for short) based on the observational data. Here “−1”, “0” and “+1” represent the preceding, simultaneous and following

years, respectively. Figure 2 displays the seasonal evolution of SST anomalies from spring to the following winter regressed upon the preceding winter NPO index. Figure 3 shows the corresponding anomalies of 850-hPa winds and precipitation. Here, the NPO index is defined as the principal component (PC) time series corresponding to the second EOF mode of SLP anomalies over the extratropical North Pacific (20°–60°N, 120°E–120°W) in the observation and CanESM2 simulations. Results obtained in this study are not sensitive to reasonable changes of the domain employed in the EOF analysis. The positive NPO phase corresponds to an anomalous cyclone and negative SLP anomalies over the subtropics and an anomalous anticyclone and positive SLP anomalies over the northern portion of the North Pacific (Fig. 1).

Evolutions of the winter NPO associated SST, 850-hPa wind, and precipitation anomalies presented in Figs. 2 and 3 are well consistent with previous studies (Vimont et al. 2001, 2003a; Alexander et al. 2010; Park et al. 2013). During a positive phase of the winter NPO, a pronounced tripole SST anomaly pattern is seen in the North Pacific in following spring, with significant negative SST anomalies in the subtropical western-central North Pacific along 20°–40°N and marked positive SST anomalies in the mid-latitudes along 40°–50°N and tropical central Pacific with a northeastward extension to the subtropical northeastern Pacific (Fig. 2a). This winter NPO-related tripole SST anomaly pattern bears

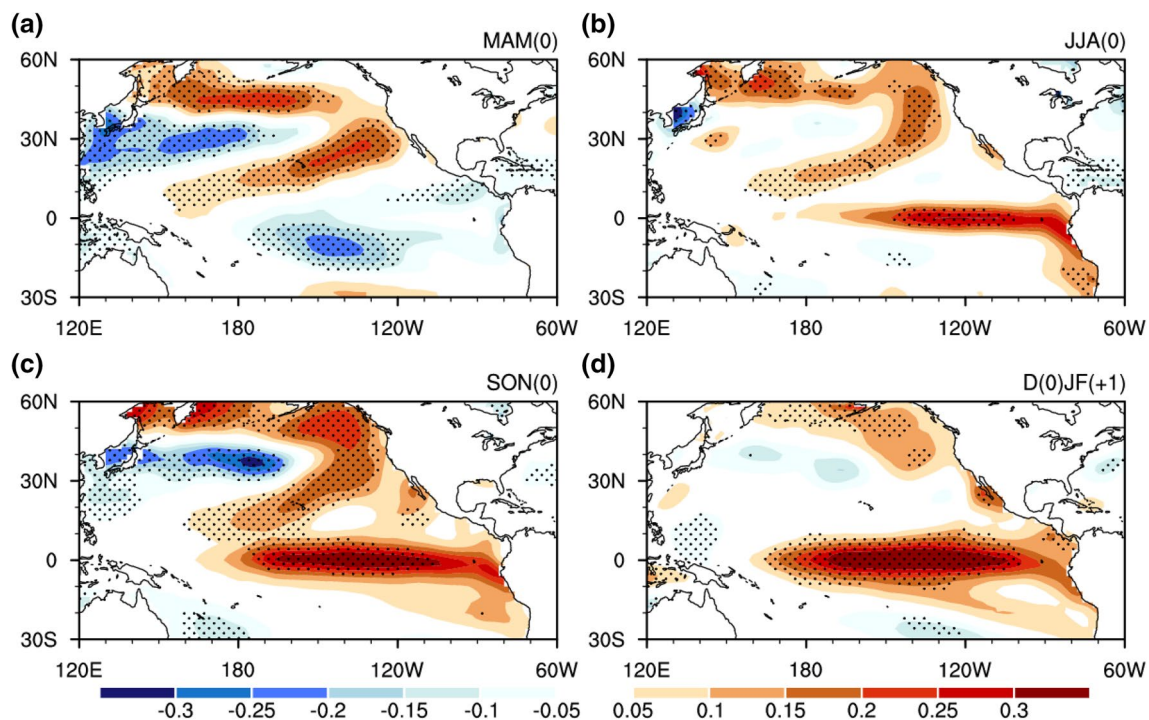


Fig. 2 Anomalies of SST (unit: °C) at **a** MAM(0), **b** JJA(0), **c** SON(0) and **d** D(0)JF(+1) regressed upon the normalized ND(−1)JFM(0) NPO index during 1951–2014 based on the observational data. Stippling regions in **a–d** indicate SST anomalies significant at the 5% level

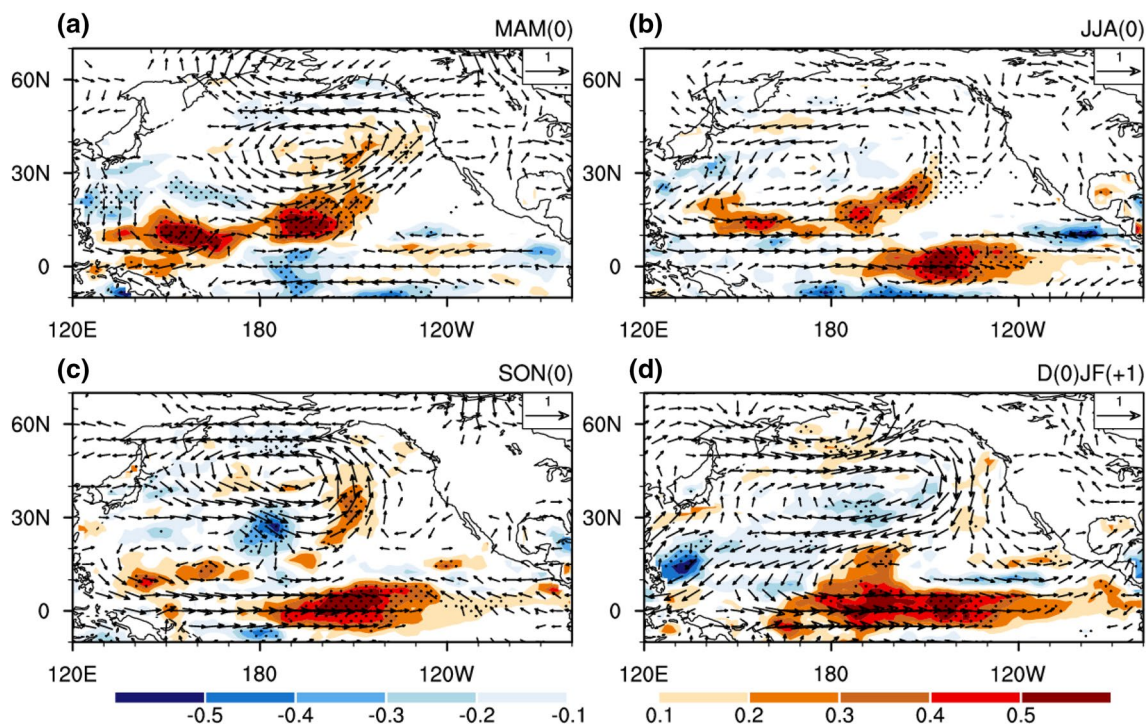


Fig. 3 As in Fig. 2, but for precipitation (shading, unit: mm day^{-1}) and 850-hPa wind (vectors, unit: m s^{-1}) anomalies. Stippling regions indicate precipitation anomalies significant at the 5% level. Wind anomalies in both directions less than 0.2 m s^{-1} are omitted

some resemblances to those associated with the Pacific Meridional mode (Chiang and Vimont 2004) and the spring Arctic Oscillation (Nakamura et al. 2006, 2007; Chen et al. 2014, 2018a). Significant negative SST anomalies can also be seen in the tropical southern Pacific around 5° – 20°S and 120° – 170°W . As demonstrated in Vimont (2001, 2003a), the formation of the spring SST anomalies in the North Pacific is attributed to the surface heat flux changes induced by the atmospheric circulation anomalies related to the winter NPO. The significant spring SST warming in the tropical North Pacific (Fig. 2a) is accompanied by pronounced positive precipitation, indicating enhanced atmospheric heating (e.g. Yu and Zwiers 2007; Chen et al. 2014), which can induce and maintain the westerly wind anomalies over the tropical western Pacific (Fig. 3a) via a Gill-type atmospheric response (Gill, 1980). As demonstrated in previous studies, westerly wind anomalies over the tropical western Pacific are a crucial trigger for the outbreak of an El Niño event (Huang et al. 2001; Vimont et al. 2001, 2003a; Lengaigne et al. 2004; Nakamura et al. 2006; Chen et al. 2014). As such, positive SST anomalies are formed in the equatorial central-eastern Pacific in the following summer (Fig. 3b). Subsequently, through the Bjerknes positive air-sea feedback mechanism, the SST warming, positive precipitation, and westerly wind anomalies over the tropical Pacific maintain and develop into the following winter (Figs. 2b–d, 3b–d). An El Niño-like SST pattern is eventually induced

in the following winter (Fig. 2d). The above process briefly describes the so-called seasonal footprinting mechanism (Vimont et al. 2001, 2003a; Alexander et al. 2010) for the NPO-ENSO connection.

For CanESM2 simulations, we first examine their ability in simulating the spatial structure of the winter NPO. Figure 4 shows regression maps of the winter SLP anomalies onto the normalized simultaneous winter NPO index for the 50 CanESM2 ensemble members. The meridional dipole pattern of SLP anomalies over the North Pacific can be well reproduced by all of the simulations, with pronounced negative anomalies over the subtropics and positive anomalies over mid-latitudes of the North Pacific. The MME result (Fig. 4, lower right) is in good agreement with that in the observation (Fig. 1b), although the center of negative SLP anomalies shifts slightly southward. Nevertheless, there exists spreads in the spatial distribution and amplitude of SLP anomalies among the 50 members. For example, members 6, 21, 40, 47 and 49 show significant negative SLP anomalies over the Russian Far East and East Asia, which are different from those in the other members. Amplitudes of negative SLP anomalies over the subtropics are also relatively weaker in members 1, 13, 31, 38, and 49 compared to the others.

To quantitatively assess the performance of the winter NPO pattern over the North Pacific simulated by the 50 members, the spatial standard deviations and correlation

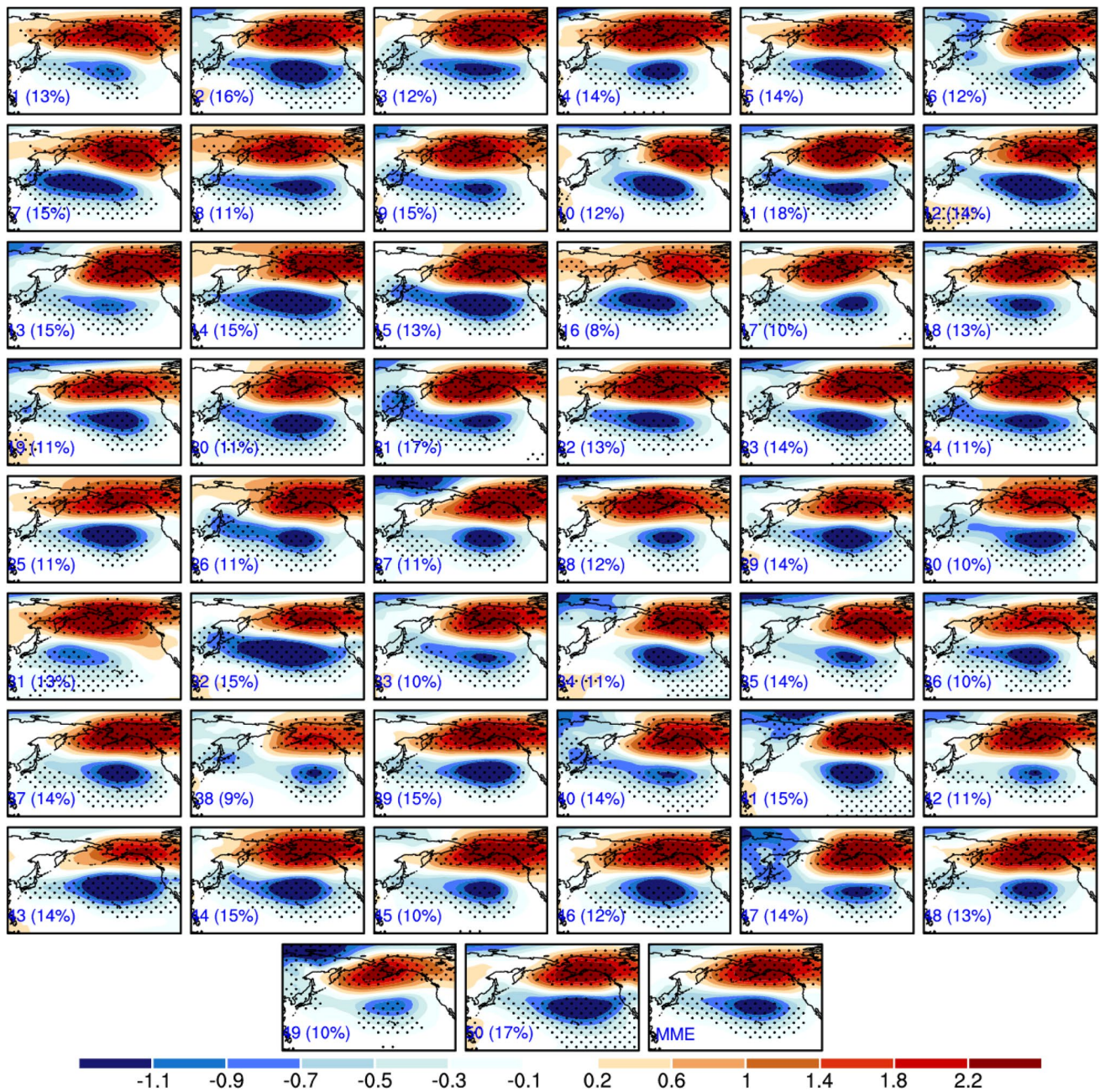


Fig. 4 ND(-1)JFM(0) SLP anomalies (unit: hPa) regressed upon the normalized ND(-1)JFM(0) NPO index for each of the CanESM2 50 members. MME indicates the average over the 50 members. Stip-

pling regions indicate anomalies significant at the 5% level. Value in the parenthesis in bottom-left indicates the explained variance of the NPO mode for each of the 50 members

coefficients of winter SLP anomalies over the North Pacific (20° – 60° N, 120° E– 120° W) are presented in a Taylor diagram in Fig. 5. Here, the ratio of spatial standard deviations for the 50 members against the observed one is calculated and presented. It is shown that the pattern correlation coefficients are larger than 0.65, confirming that the CanESM2 simulations can well reproduce the observed winter NPO pattern. However, most of the simulations overestimate the spatial standard deviation of SLP anomalies over the North

Pacific. The MME mean has a better performance than most members in simulating both the spatial standard deviation (the standard deviation for MME is about 1.1) and spatial pattern correlation (the pattern correlation for MME is about 0.93) of the winter NPO.

We then evaluate the connection of the winter NPO with its subsequent winter ENSO in the 50-member simulations. Figure 6 shows regression maps of winter (D(0)JF(+1)) SST anomalies onto the normalized preceding winter (ND(-1)

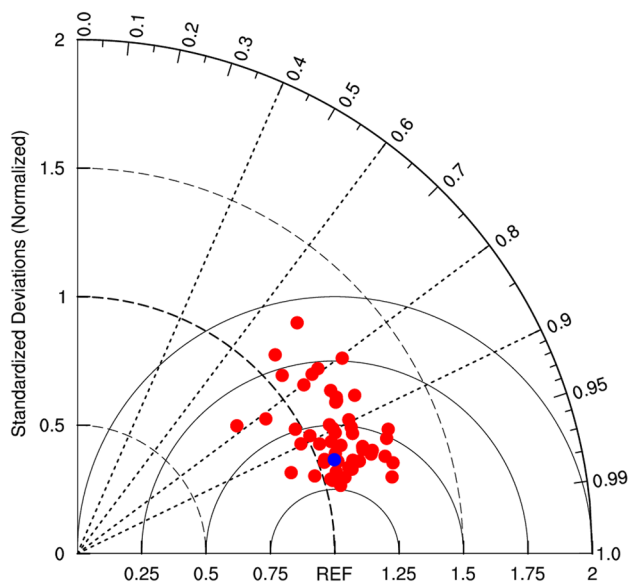


Fig. 5 Taylor diagram of ND(-1)JFM(0) SLP anomalies over the extratropical North Pacific (20° – 60° N, 120° E– 120° W) presented in Fig. 4, with respect to the observation. The blue dot represents the MME result

JFM(0)) NPO index over the period of 1951–2004 for each of the 50 members and their MME mean. Figure 7 gives correlation coefficients between the ND(-1)JFM(0) NPO index and D(0)JF(+1) Niño-3.4 index for individual members and the MME. The Niño-3.4 index is usually employed to represent ENSO variability in previous studies, which is defined as the regional mean SST anomalies over the region (5° S– 5° N, 120° – 170° W). Most members, as well as the MME, can produce an El Niño-like SST pattern in the tropical Pacific in winter when the preceding winter NPO is in its positive phase (Fig. 6). Figure 7 further indicates that 30 members can produce the observed significant correlation of the winter NPO with the following winter ENSO, whereas the winter NPO-ENSO relations are not statistically significant in other 20 members. The correlation coefficients for MME is about 0.34, significant at the 5% level, comparable to the observed value 0.36 over the same period (Fig. 7). The observed correlation between the two indices is also within the simulated error bar as shown in Fig. 7. Hence, most of the 50 simulations and their ensemble mean can reasonably well simulate the winter NPO-ENSO linkage. In addition, it is noted that centers of the SST anomalies for the MME and most simulations are in the central Pacific. This is also consistent with previous findings (Yu and Kim 2011; Yu et al. 2012) that the winter NPO is an important extratropical forcing on the Central Pacific (CP)-type ENSO (also called ENSO Modoki, Ashok et al. 2007).

An immediate question following the NPO-ENSO connection is whether the observed SFM process can also be

simulated by this climate model? To address this, we examine seasonal evolutions of the SST, 850-hPa wind, precipitation, and surface heat flux anomalies regressed upon the normalized winter NPO index. Figures 8, 9, and 10 present the MME results. Since the winter surface sensible heat flux, shortwave and longwave radiation anomalies in association with the winter NPO are much weaker than the winter NPO associated surface latent heat flux anomalies, we only present the surface net heat flux and latent heat flux anomalies in Fig. 10. The surface net heat flux is the sum of shortwave and longwave radiations and latent and sensible heat fluxes at the surface. In general, MME can reasonably well reproduce the seasonal footprinting mechanism related to the winter NPO (Figs. 8, 9 and 10; Vimont et al. 2003a). Specifically, a dipole atmospheric circulation anomaly pattern appears in the North Pacific in winter during a positive NPO phase, with an anomalous anticyclone over mid-latitudes and an anomalous cyclone over the subtropics (Fig. 9a). Accordingly, significant positive precipitation anomalies are seen around 130° – 170° W and 20° – 40° N, and negative precipitation anomalies are found around the Aleutian region (Fig. 9a, color shading). The centers of positive and negative precipitation anomalies over the North Pacific collocate with the centers of the anomalous cyclone and anticyclone, respectively. The winter SST anomalies are featured by a tripole pattern, with significant positive anomalies in the mid-latitude North Pacific around 40° – 50° N and in the subtropical North Pacific with much weaker amplitude, accompanied by negative anomalies over the western North Pacific around 30° N (Fig. 8a). The tripole SST anomalies largely enhance in the following spring (Fig. 8b). The winter net surface heat flux anomalies, which are dominated by surface latent heat flux anomalies, are also featured by a tripole anomaly pattern over the North Pacific (Fig. 10a, f). This suggests that the formation of the tripole SST anomaly pattern in North Pacific is mainly attributed to the surface heat flux changes induced by the atmospheric circulation anomalies in association with the winter NPO, consistent with the observed results (Vimont et al. 2001, 2003a). In particular, the strong southwesterly wind anomalies over the subtropical North Pacific reduce the northeasterly winds and contribute to SST warming there (Fig. 8a) via reducing surface wind speed (not shown) and a reduction of upward latent heat flux (Fig. 10b) (Vimont et al. 2001, 2003a). Easterly wind anomalies over the mid-latitude North Pacific around 40° – 60° N are opposite to the climatological westerly winds, resulting in SST warming there via decrease in the upward latent heat flux (Fig. 10b). In addition, the anomalous easterly winds could lead to a northward movement of warmer water from lower latitudes via Ekman transportation (Wu and Kinter 2010), which also contribute partly to SST warming in mid-latitudes. The significant northerly wind anomalies over the western Pacific carry colder air from

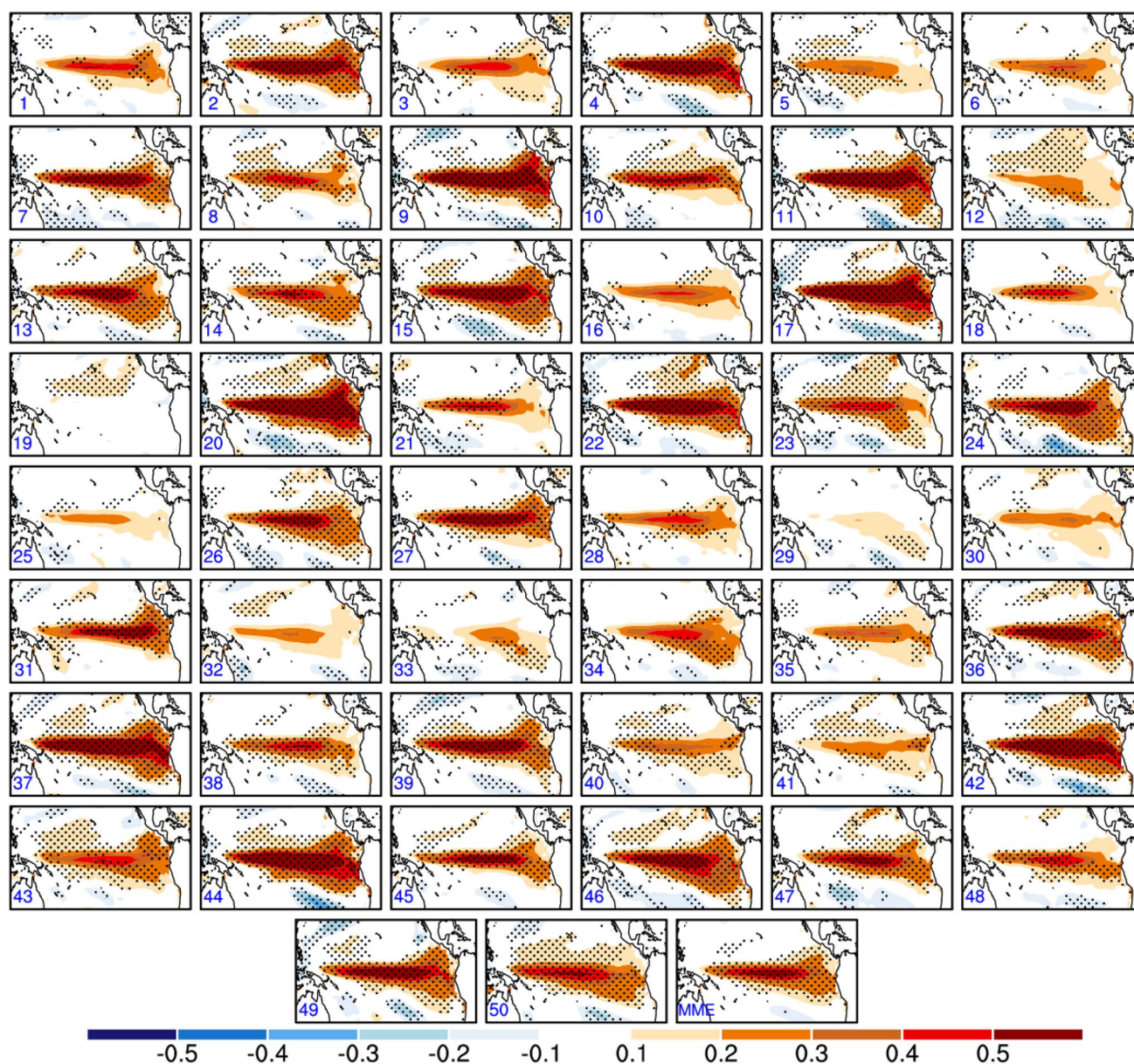


Fig. 6 D(0)JF(+1) SST (unit: °C) anomalies regressed upon the normalized ND(-1)JFM(0) NPO index during 1951–2004 for each of the CanESM2 50 members and their MME. Stippling regions indicate SST anomalies significant at the 5% level

higher latitudes, increase the sea-air humidity difference and lead to increase in upward latent heat flux and SST cooling (Fig. 10a, f). The surface heat flux anomalies become weak over the extratropical North Pacific after spring (Fig. 10b–e, g–j). Meanwhile, the tropical central-eastern Pacific is dominated by negative net heat flux anomalies from spring to following winter (Fig. 10b–e, g–j). This suggests that the oceanic dynamic plays an important role in the development and maintenance of the positive SST anomalies in the tropical central-eastern Pacific.

It should be mentioned here that positive SST anomalies can also be seen in the equatorial central Pacific during

spring in the MME (Fig. 8b), which is different from the observation (Fig. 2a). This is likely because the cyclonic anomaly and negative SLP anomalies over the subtropical North Pacific and the related westerly wind anomalies to their south flank are located more southward in the MME compared to the observed as described above (Figs. 1b, 9a). The winter westerly wind anomalies in the tropical western Pacific in the MME (Fig. 9a) can directly contribute to SST warming in the equatorial central Pacific in the following spring (Fig. 8b) via triggering an eastward propagating warm Kelvin wave (Jin 1997; Huang et al. 2001; Nakamura et al. 2006; Chen et al. 2014). In addition, pronounced positive

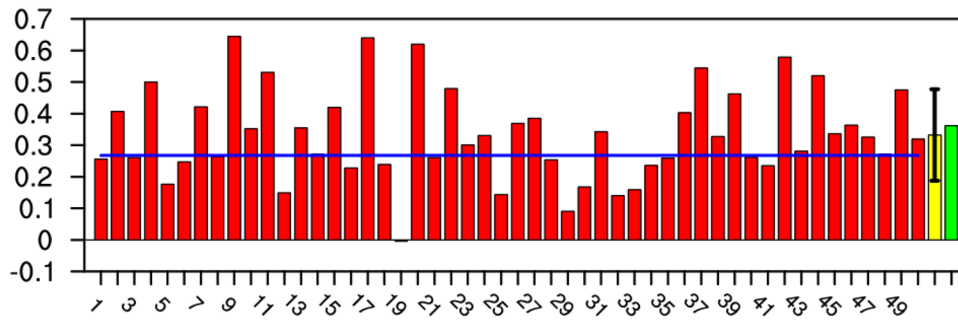


Fig. 7 Correlation coefficients between the winter NPO index and its following winter Niño3.4 index during 1951–2004. The blue line indicates the correlation coefficient that is significant at the 5% level

over the 55 winters. Yellow bar indicates the MME result. The error bar indicates one standard deviation of the correlation coefficients among the 50 members. The green bar represents the observed result

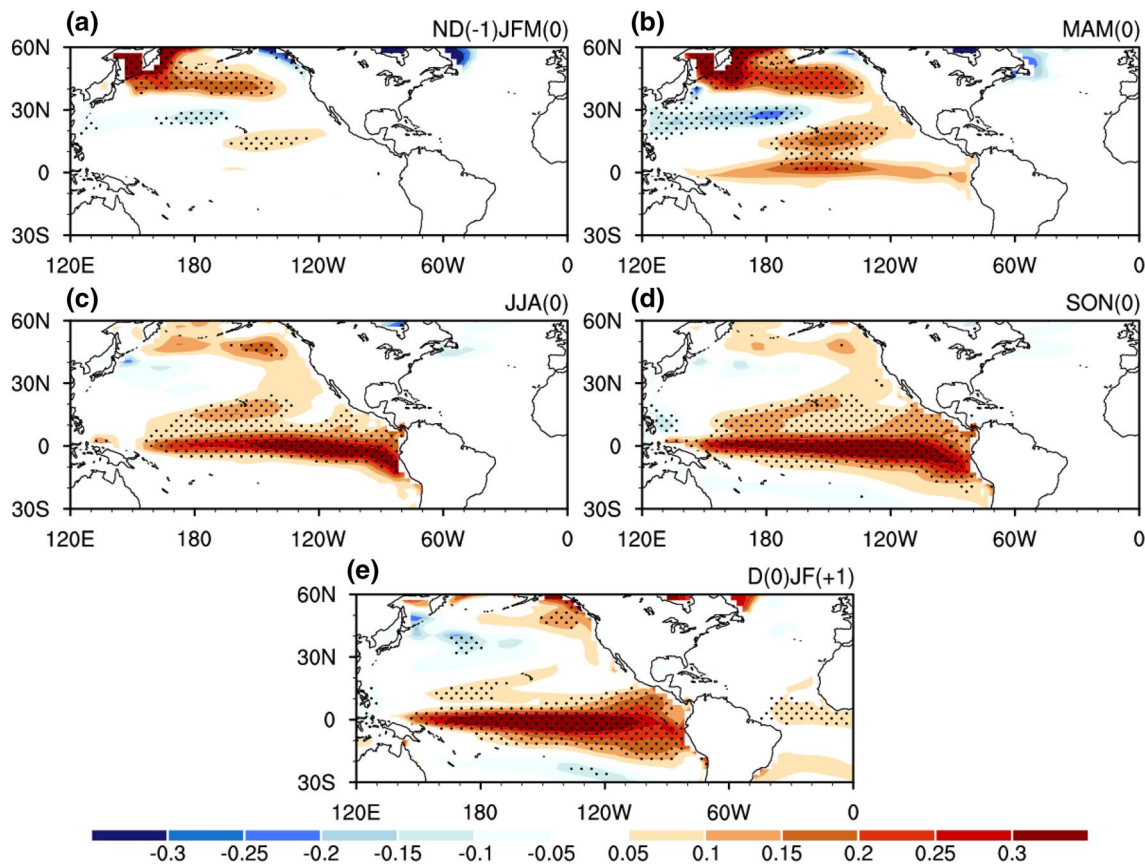


Fig. 8 Ensemble means of the SST (unit: °C) anomalies at **a** ND(-1)JFM(0), **b** MAM(0), **c** JJA(0), **d** SON(0), and **e** D(0)JF(+1) regressed upon the preceding ND(-1)JFM(0) NPO index for the CanESM2 50 members. Stippling regions indicate SST anomalies significant at the 5% level

precipitation anomalies are seen in spring over the tropical central Pacific in association with significant SST warming there (Figs. 8b, 9b). These positive precipitation anomalies (indicating increase in atmospheric heating) play an important role in generating and maintaining westerly wind anomalies over the tropical western Pacific as indicated by Vimont et al. (2003a) (Fig. 9b). The tropical western Pacific westerly wind anomalies would, in turn, further contribute

to SST warming and positive precipitation anomalies in the tropical central-eastern Pacific (Figs. 8b–e, 9b–e). Through the Bjerknes positive air-sea feedback mechanism, an El Niño-like event would eventually be generated in the following winter (Fig. 8e). Overall, the seasonal footprinting mechanism connecting the winter NPO with its following winter ENSO can be reasonably well captured in the MME of the 50 CanESM2 members.

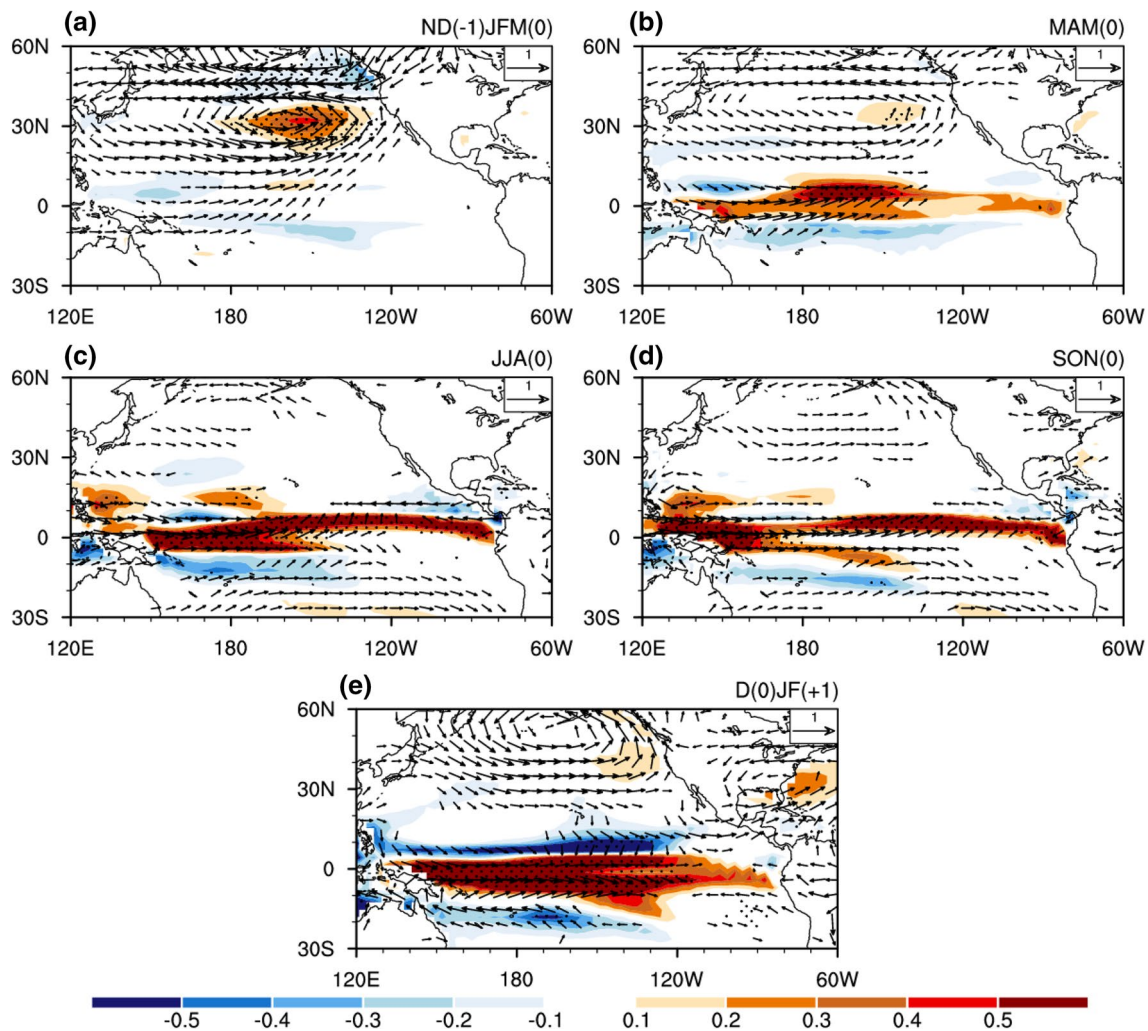


Fig. 9 Ensemble means of the precipitation (shading; unit: mm day^{-1}) and 850-hPa wind (vectors; unit: m s^{-1}) anomalies at **a** ND(-1)JFM(0), **b** MAM(0), **c** JJA(0), **d** SON(0), and **e** D(0)JF(+1)

Previous studies have demonstrated that spring (February–March–April-average, FMA) SST anomalies in the northern tropical Atlantic (NTA) have a significant impact on the following winter ENSO events (Ham et al. 2013; Ham and Kug 2015). A relevant question is: whether the winter NPO-ENSO relation simulated by the CanESM2 is influenced by the spring NTA SST? Figure 8 indicates that the MME SST anomalies associated with the winter NPO are weak and statistically insignificant in the NTA region. This suggests that the winter NPO has a weak relation with the spring SST anomalies in the NTA for the MME of the 50 members. Furthermore, a spring NTA SST index is defined as the area-averaged SST anomalies over the region of 0° – 15°N and 90°W – 20°E following Ham et al. (2013). Correlation coefficients between the winter NPO index and its following spring NTA SST index during 1951–2004 for the 50 members are weak and statistically insignificant

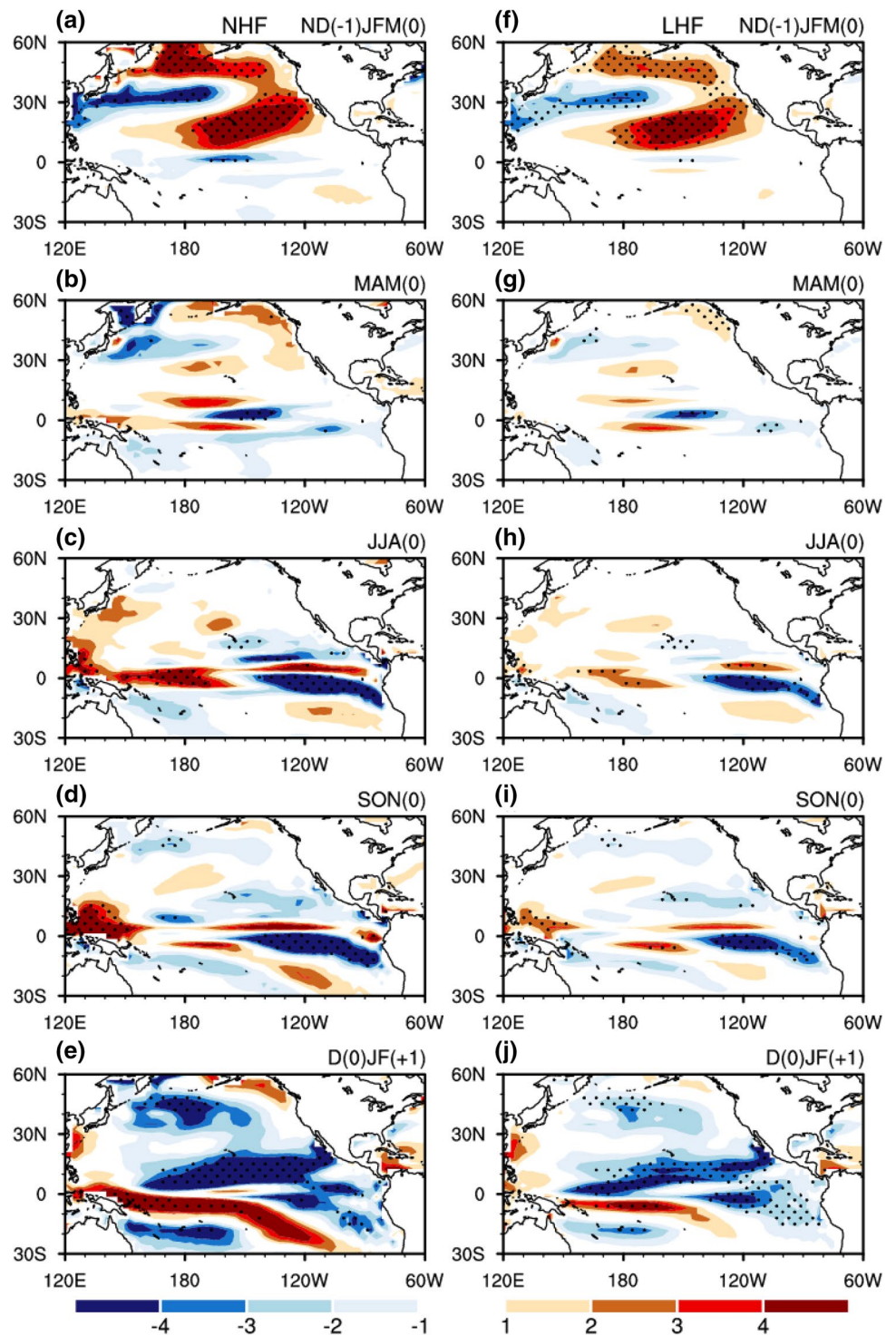
regressed upon the preceding ND(-1)JFM(0) NPO index for the CanESM2 50 members. Stippling regions indicate precipitation anomalies significant at the 5% level

(not shown). These evidences suggest that the winter NPO-ENSO relation is not likely influenced by the spring NTA SST anomalies. The winter NPO and spring NTA SST tend to be two independent factors for the following winter ENSO occurrence. Nevertheless, the combined impact of the winter NPO and spring NTA SST on the following winter ENSO is worthy of further investigation.

4 Diversity of the winter NPO-ENSO relations among ensemble members

The above analysis indicates that there is a large spread of the winter NPO-ENSO relationship among the 50 ensemble members (Fig. 7). In particular, member 19 even produces a slightly negative correlation coefficient between the winter NPO index and subsequent winter Niño3.4

Fig. 10 Ensemble means of the net surface heat flux (unit: $W m^{-2}$) anomalies at **a** ND(-1) JFM(0), **b** MAM(0), **c** JJA(0), **d** SON(0), and **e** D(0)JF(+1) regressed upon the preceding ND(-1)JFM(0) NPO index for the 50 members. **f-j** As in **a-e**, but for the surface latent heat flux anomalies. Stippling regions indicate anomalies significant at the 5% level



index. Additionally, the correlation coefficients in 20 out of the 50 members cannot pass the 95% confidence level. As these simulations are forced by the same external forcing, the spread in the NPO-ENSO relation among different ensemble members is due solely to the internal climate variability. In the following, we further explore the diversity of simulated NPO-ENSO relations by comparing ten

ensemble members with highest NPO-ENSO correlations (denoted as HC members) and ten ensemble members with lowest NPO-ENSO correlations (denoted as LC members) selected based on Fig. 7. Results reported here are not sensitive to slight changes of the selected members employed in the HC and LC composites.

Figure 11 shows the ensemble means of $D(0)JF(+1)$ SST, 850-hPa wind, and precipitation anomalies regressed upon the preceding winter NPO index for the HC and LC members, as well as their differences. Ensemble means of the SST, precipitation and 850-hPa wind anomalies for the HC members display a significant El Niño-like pattern (Fig. 11a, d). Pronounced SST warming is seen in the tropical central-eastern Pacific and off the west coast of Canada, accompanied by SST cooling in the subtropical-midlatitude

North Pacific (Fig. 11a). Correspondingly, significant positive precipitation and westerly wind anomalies occur in the tropical Pacific (Fig. 11d). In addition, a strong cyclonic anomaly is seen over the mid-latitude North Pacific, indicating an enhanced Aleutian Low in winter (Fig. 11d). By contrast, for the ensemble mean of the LC members, SST warming is also seen in the tropical Pacific (Fig. 11b), while its amplitude is much weaker and significantly different from the HC counterpart (Fig. 11c). Similarly, precipitation and

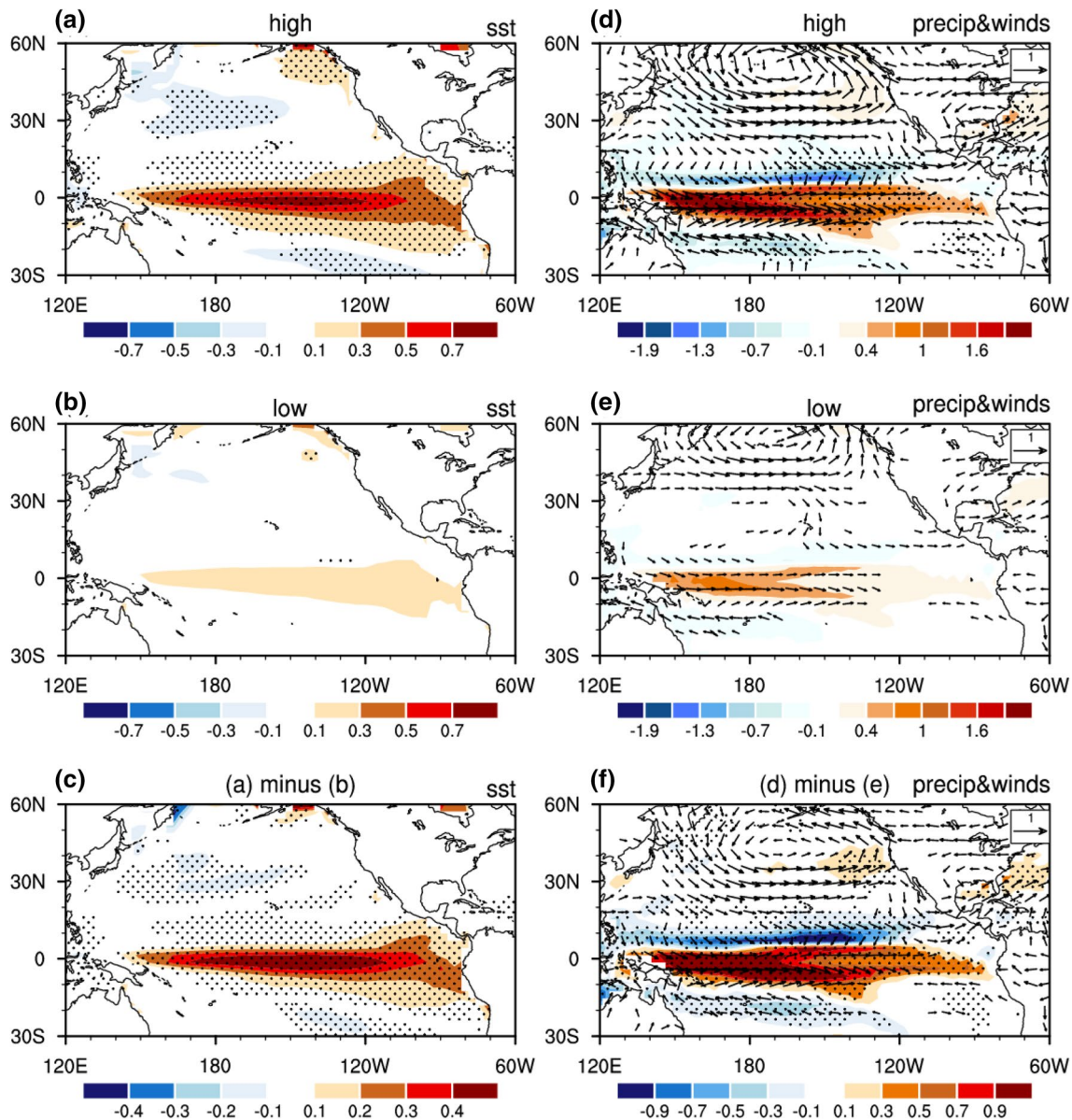


Fig. 11 Ensemble means of $D(0)JF(+1)$ **a, b** SST (unit: $^{\circ}\text{C}$), **d, e** precipitation (shading; unit: mm day^{-1}) and 850-hPa wind (vectors; unit: m s^{-1}) anomalies regressed upon the $\text{ND}(-1)\text{JFM}(0)$ NPO index for the HC and LC members. Definitions of the HC and LC members are described in the text. Stippling regions in **a, b** and **d, e** indicate SST and precipitation anomalies significant at the 5% level, respectively.

Wind anomalies in both directions less than 0.2 m s^{-1} are omitted in **d, e**. **c** The differences between **a** and **b**. **f** The differences between **d** and **e**. Stippling regions in **c** and **f** indicate the differences in SST and precipitation that are significantly different from zero at the 5% level, respectively

wind anomalies over the tropical Pacific for the LC members are also much weaker than those for the HC members (Fig. 11d–f).

To further compare the physical processes related to the NPO-ENSO relation in the HC and LC composites, we calculate ensemble means of the ND(–1)JFM(0) SLP, SST and 850-hPa wind anomalies regressed upon the winter NPO index for the HC and LC members (Fig. 12) and the ensemble means of these anomalies in the following spring (Fig. 13). The spatial distributions of the ND(–1)

JFM(0) SLP, 850-hPa wind and SST anomalies over the North Pacific are broadly similar between the HC and LC members. In particular, SLP and 850-hPa wind anomalies both show a meridional dipole pattern (Fig. 12a, b, d, e), and the SST anomalies feature a meridional tripole pattern (Fig. 13a, b, d, e). However, different maps of the winter SLP, 850-hPa wind and SST anomalies between the HC and LC members (Figs. 12c, f, 13c, f) indicate that there exist large differences in the winter SLP anomalies over the subtropical North Pacific (blue box regions in Fig. 12a–c). In

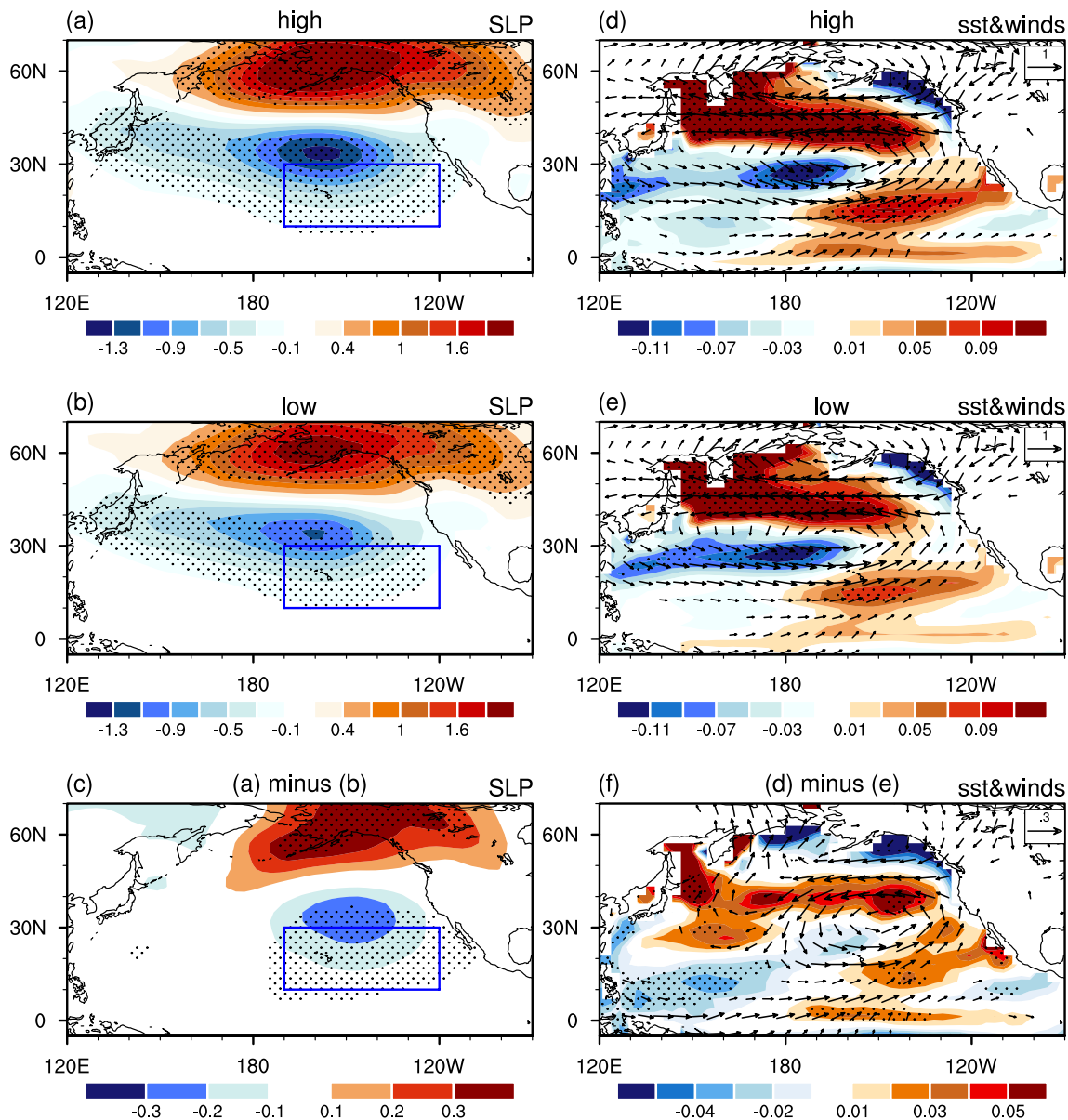


Fig. 12 Ensemble means of ND(–1)JFM(0) (a, b) SLP (unit: hPa), (d, e) SST (shading; unit: °C) and 850-hPa wind (vectors; unit: $m s^{-1}$) anomalies regressed upon the ND(–1)JFM(0) NPO index for the HC and LC members. Stippling regions in a, b and d, e indicate SLP and precipitation anomalies significant at the 5% level, respectively.

Wind anomalies in both directions less than $0.2 m s^{-1}$ are omitted in d, e. c The differences between a and b. f The differences between d and e. Stippling regions in c and f indicate the differences in SLP and precipitation that are significantly different from zero at the 5% level, respectively

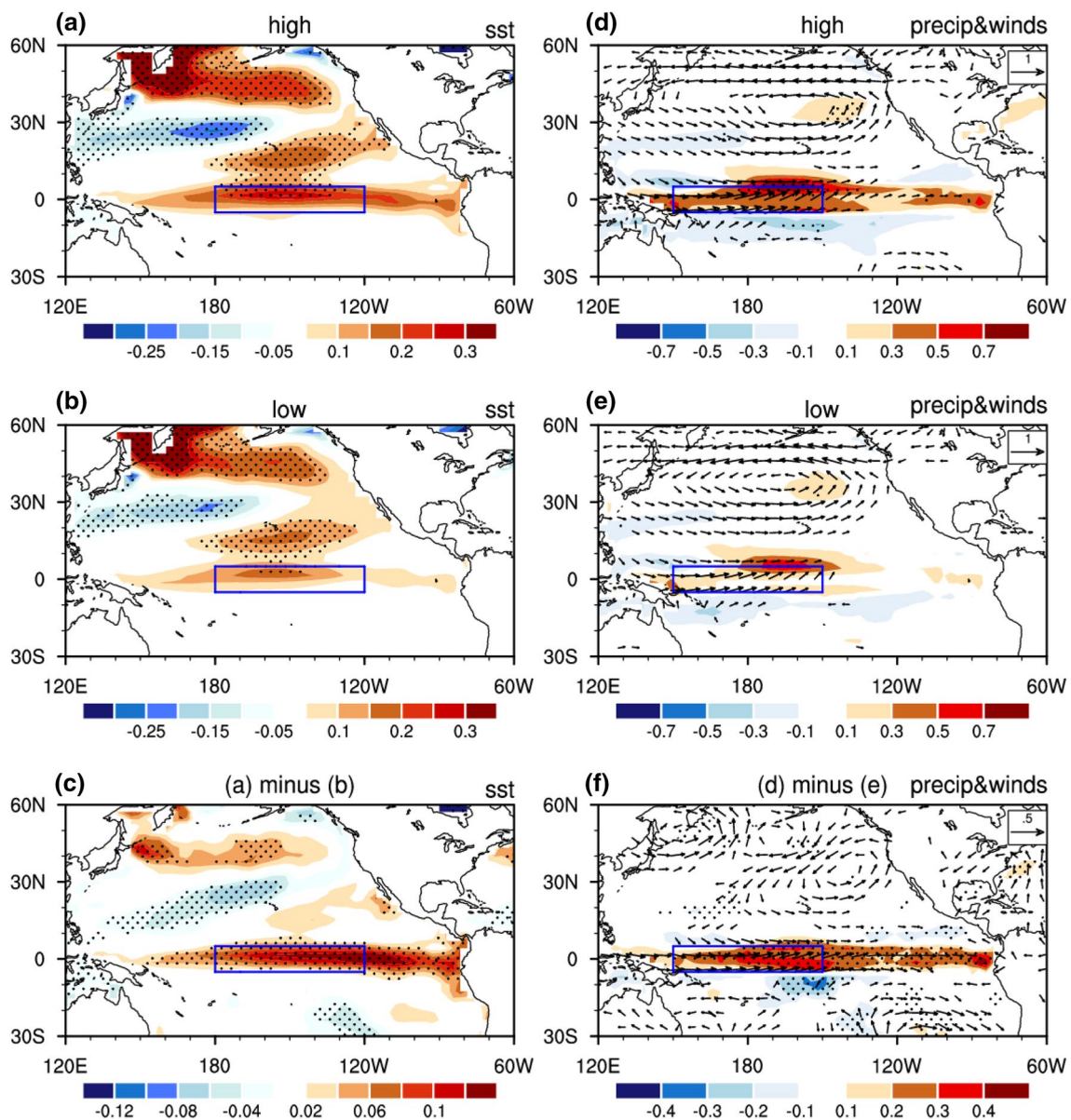


Fig. 13 Ensemble means of MAM(0) (a, b) SST (unit: °C), d, e precipitation (shading; unit: mm day⁻¹) and 850-hPa wind (vectors; unit: m s⁻¹) anomalies regressed upon the ND(-1)JFM(0) NPO index for the HC and LC members. Stippling regions in a, b and d, e indicate SST and precipitation anomalies significant at the 5% level, respectively.

particular, amplitudes of the negative SLP anomalies over the subtropical North Pacific are much larger in the HC than LC members (Fig. 12c). The positive SLP anomalies are also stronger over the mid-latitude North Pacific, where NPO's northern center locates, in the HC than LC members. This suggests that the members with a closer winter NPO-ENSO relation tend to have a stronger amplitude of NPO (Fig. 12c). In addition, it can be seen from Fig. 13 that the positive SST and precipitation anomalies in the tropical central Pacific, as well as the anomalous westerly winds over the tropical

western Pacific are also much stronger for the HC than LC members in spring (Fig. 13c, f). In general, the intensity differences in the winter SLP anomalies over the subtropical North Pacific between the two composites are similar to the differences in the winter SST anomalies in the subtropical North Pacific, and to the differences of the SST, precipitation and westerly wind anomalies over the tropical Pacific in the following spring.

The above results suggest that the spread of the winter NPO-ENSO relations among the ensemble members is due

essentially to the diversity of the intensity of the winter NPO. Specifically, strong negative SLP and cyclonic anomalies in ND(-1)JFM(0) over the subtropical North Pacific would lead to strong SST warming there in the simultaneous winter, as well as stronger SST warming and positive precipitation anomalies in the tropical central Pacific, accompanied by strong westerly wind anomalies over the tropical western Pacific in the following spring. These anomalies sustain in the following seasons (not shown), leading to strong El Niño events in the following winter.

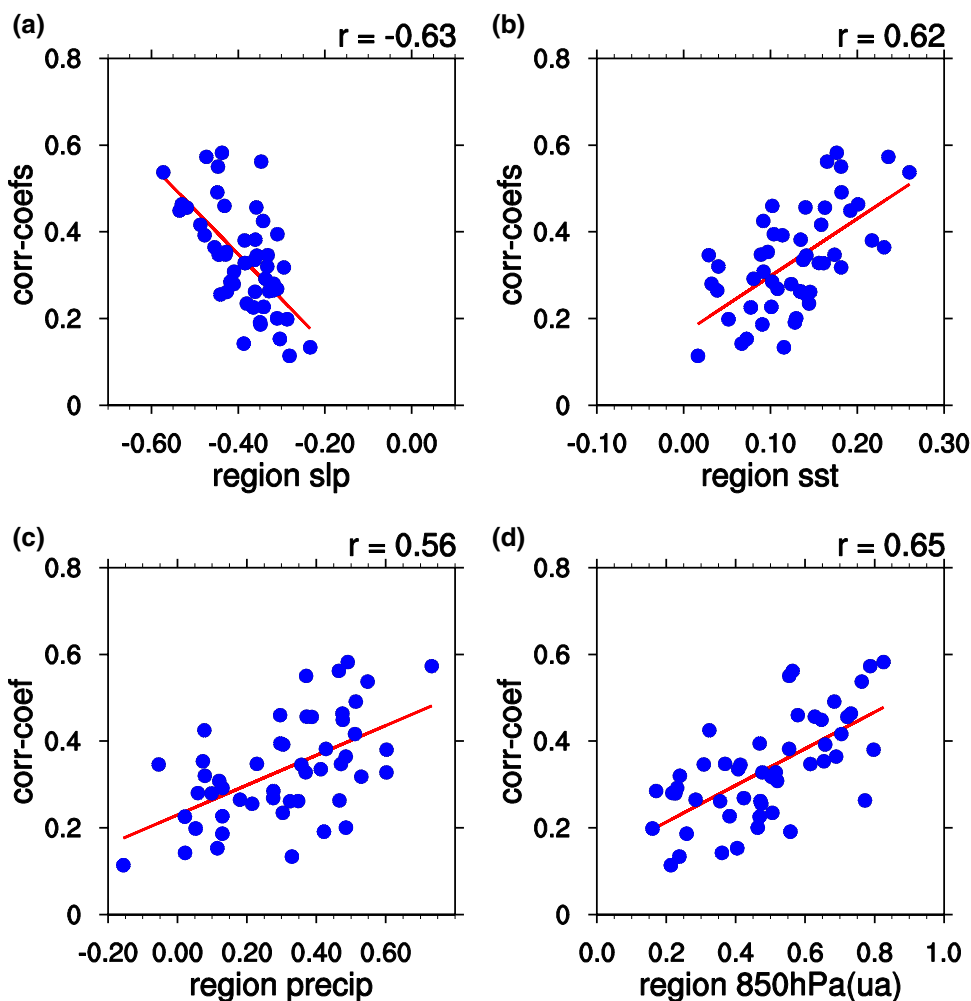
To further confirm the above relationships, we present scatter plots of the correlation coefficient between the ND(-1)JFM(0) NPO and D(0)JF(+1) Niño3.4 indices (Fig. 7) versus the ND(-1)JFM(0) regional mean SLP anomalies over the subtropical North Pacific (blue box in Fig. 12a-c) among the 50 members in Fig. 14a. It is clear from Fig. 14a that the ensemble members with strong ND(-1)JFM(0) SLP anomalies over the subtropical North Pacific tend to have large positive correlations between the ND(-1)JFM(0) NPO and D(0)JF(+1) Niño3.4 indices. The two quantities presented in Fig. 14a have a mean correlation

of -0.63 among the 50 ensemble members, significant at the 99% confidence level.

Figure 14a-c shows scatter plots of the correlation coefficient between the ND(-1)JFM(0) NPO and D(0)JF(+1) Niño3.4 indices versus the regional mean MAM(0) SST and precipitation anomalies in the tropical central Pacific (blue box in Fig. 13a-c) and the regional mean MAM(0) 850-hPa zonal wind anomalies over the tropical western-central Pacific (blue box in Fig. 13d-f) among the 50 members, respectively. The correlation coefficients between the two quantities considered in Fig. 14b-d are also statistically significant at the 99% confidence level. Overall, the above analysis suggests that internal climate variability would influence the SFM process related to the winter NPO-ENSO relationship through modulating the subtropical center of the wintertime NPO.

As indicated by Vimont et al. (2003a), surface westerly wind anomalies over the tropical western-central Pacific play an important role in the formation and maintenance of the positive SST anomalies in the tropical central-eastern Pacific via triggering eastward propagating and downwelling

Fig. 14 Scatter plots of the correlation coefficients between the ND(-1)JFM(0) NPO and D(0)JF(+1) Niño3.4 indices versus **a** the regional mean ND(-1)JFM(0) SLP anomalies over the subtropical North Pacific (blue box in Fig. 12a-c), **b** the regional mean MAM(0) SST anomalies in the tropical central Pacific (blue box in Fig. 13a-c), **c** the regional mean MAM(0) precipitation anomalies in the tropical central Pacific (blue box in Fig. 13a-c), and **d** the regional mean MAM(0) 850-hPa zonal wind anomalies in the tropical western-central Pacific (blue box in Fig. 13d-f) among the 50 members



warm Kelvin waves. Figure 15a, b display the ensemble means of the evolutions of equatorial Kelvin wave forcing anomalies regressed upon the winter NPO index for the HC and LC members, respectively. As demonstrated in previous studies (Battisti 1988; Vimont et al. 2003a), positive (negative) values of KWF indicate that surface zonal wind stress anomalies induce eastward propagating and downwelling (upwelling) equatorial Kelvin waves that lead to

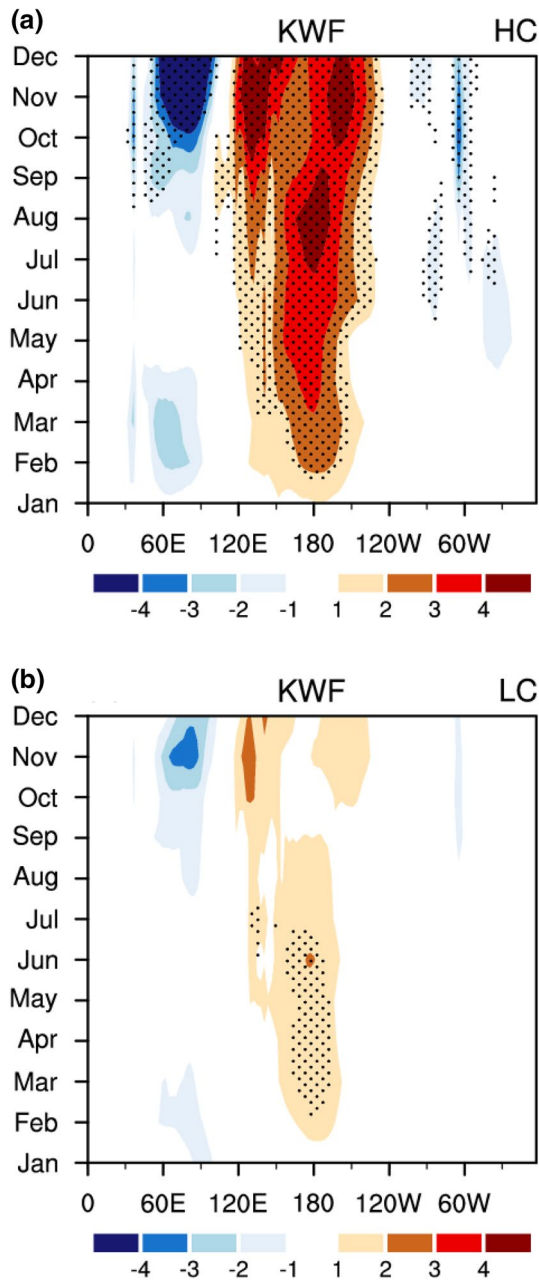


Fig. 15 Ensemble means of the evolution of equatorial Kelvin wave forcing anomalies (unit: $10^3 \times \text{N m}^{-2}$) regressed upon the ND(-1) JFM(0) NPO index for the **a** HC and **b** LC members. Stippling regions indicate anomalies significant at the 5% level, respectively

SST warming (cooling). For the HC members, significant and positive KWF anomalies are seen over the tropical western-central Pacific in early spring (Fig. 15a). These positive KWF anomalies maintain and develop in the following autumn–winter (Fig. 15a), which contribute to an El Niño-like SST warming in the tropical central-eastern Pacific (Fig. 11a). Hence, low-level westerly wind anomalies over the tropical western-central Pacific contribute to SST warming in the tropical central-eastern Pacific via triggering eastward propagating warm Kelvin waves for the HC members. By contrast, for the LC members, the KWF anomalies are much weaker and less significant (Fig. 15b). Therefore, the winter NPO cannot lead to an El Niño-like SST warming in the tropical central-eastern Pacific (Fig. 11b).

In addition, low-level westerly wind anomalies over the tropical western Pacific can also lead to SST warming in the tropical central-eastern Pacific via the zonal advection effect (e.g., An and Jin 2001). In particular, low-level westerly wind anomalies bring warmer water eastward from the western Pacific warm pool, and contribute to SST warming in the tropical central-eastern Pacific. Thus, the stronger spring low-level westerly wind anomalies over the tropical western Pacific (Fig. 13d, e) in association with the preceding winter NPO for the HC members also contribute to subsequent larger SST warming in the tropical central-eastern Pacific (Fig. 11a, b) via the zonal advection effect compared to that for the LC members.

It should be mentioned that we have also examined the difference of the climatological mean SST between the HC and LC members. Differences in the mean SST between the HC and LC members are weak from ND(-1)JFM(0) to D(0)JF(+1) over most parts of the Pacific Ocean (not shown). This suggests that the divergence of the winter NPO-ENSO relation across the 50 members is not likely due to the spread of the climatological mean SST.

5 Summary and discussions

The NPO is an important pattern of atmospheric interannual variability over the extratropical North Pacific. Previous studies indicated that the boreal winter NPO has a notable impact on the following winter ENSO occurrence via the so-called seasonal footprinting mechanism. This study examines this NPO-ENSO connection in a 50-member large ensemble simulations conducted with the CanESM2 for the historical period of 1950–2005. We first examine the model's performance in simulating the spatial pattern of the winter NPO. The observed meridional dipole structure of atmospheric anomaly can be well reproduced by all of the 50 ensemble members. During a positive phase of the NPO, an anomalous anticyclone and positive SLP anomalies can be seen over the mid-latitude North Pacific, accompanied by

an anomalous cyclone and negative SLP anomalies over the subtropics of North Pacific. The pattern correlations of the SLP anomalies over the North Pacific between the observed and 50 simulations are larger than 0.65. Nevertheless, most of the ensemble members tend to overestimate the spatial standard deviation of the winter SLP anomalies over the North Pacific. In addition, the ensemble mean of the southern center of the winter NPO is located more equatorward than the observed result.

We then examine the winter NPO-ENSO relationship in the 50 ensemble members. Results show that MME of the 50 members can well reproduce the NPO-ENSO relationship as well as the associated SFM process. However, there exists a large spread of the winter NPO-ENSO relation among the 50 members due to internal climate variability. The correlation coefficients between the winter NPO index and its following winter Niño-3.4 index are statistically significant at the 5% level for 30 members and insignificant for the other 20 members. The diversity of the winter NPO-ENSO connection among the 50 members is found to be due to the spread in the winter SLP and associated atmospheric circulation anomalies over the subtropical North Pacific. In particular, the simulations with strong (weak) winter SLP anomalies over the North Pacific tend to produce strong (weak) SST and precipitation anomalies in the tropical central Pacific and strong (weak) westerly wind anomalies over the tropical western Pacific during the following spring. These anomalies sustain in the following seasons and eventually lead to significant (insignificant) ENSO events in the following winter. Hence, internal climate variability should be considered in linking the winter NPO to its following winter ENSO.

The present study is based on the large ensemble simulations from the CanESM2 model. One may ask whether the feature that strong NPO-ENSO correlations tend to have strong winter subtropical North Pacific atmospheric anomalies can be found in the observation. To address this question, we have examined moving correlation of the winter NPO index with the following winter Niño-3.4 index in the observation (not shown). It is found that the winter NPO-ENSO correlation is weak after the late-1960s, but has a slight recover since the mid-1980s. Then, we further select two periods with high and low correlations, respectively, based on the observed moving correlation. Results indicate that winter NPO-related simultaneous winter SLP anomalies over North Pacific both display a meridional pole over high and low correlation periods. In comparison, amplitude of the negative SLP anomalies in association with the winter NPO index is stronger over the subtropical North Pacific during high correlation period compared to low correlation period (not shown). Hence, in the observation, atmospheric anomalies over the subtropical North Pacific in winter related to the winter the NPO are stronger during high than low correlation periods.

Acknowledgements We thank the anonymous reviewers for their constructive suggestions and comments, which help to improve the paper. This study is supported by the National Natural Science Foundation of China grants (41605050, 41530425, and 41775080), and the Young Elite Scientists Sponsorship Program by the China Association for Science and Technology (2016QNRC001). We greatly appreciate the work of colleagues at the CCCma in the production of the model results analyzed here. We thank Dr. Bill Merryfield and Dr. M. Casas Prat for helpful suggestions as internal reviews of the manuscript. The NCEP-NCAR reanalysis data are obtained from <ftp://ftp.cdc.noaa.gov/Datasets/ncep.reanalysis.derived>. The ERSSTv3b data are obtained from <https://www.esrl.noaa.gov/psd/data/gridded>.

Open Access This article is licensed under a Creative Commons Attribution 4.0 International License, which permits use, sharing, adaptation, distribution and reproduction in any medium or format, as long as you give appropriate credit to the original author(s) and the source, provide a link to the Creative Commons licence, and indicate if changes were made. The images or other third party material in this article are included in the article's Creative Commons licence, unless indicated otherwise in a credit line to the material. If material is not included in the article's Creative Commons licence and your intended use is not permitted by statutory regulation or exceeds the permitted use, you will need to obtain permission directly from the copyright holder. To view a copy of this licence, visit <http://creativecommons.org/licenses/by/4.0/>.

References

- Alexander MA, Bladé I, Newman M, Lanzante JR, Lau NC, Scott JD (2002) The atmospheric bridge: the influence of ENSO teleconnections on air–sea interaction over the global oceans. *J Clim* 15:2205–2231
- Alexander MA, Vimont DJ, Chang P, Scott JD (2010) The impact of extratropical atmospheric variability on ENSO: Testing the seasonal footprinting mechanism using coupled model experiments. *J Clim* 23:2885–2901
- An SI, Jin FF (2001) Collective role of thermocline and zonal advective feedbacks in the ENSO mode. *J Clim* 14:3421–3234
- Arora VK et al (2011) Carbon emission limits required to satisfy future representative concentration pathways of greenhouse gases. *Geophys Res Lett* 38:L05805
- Ashok K, Behera SK, Rao SA, Weng H, Yamagata T (2007) El Niño Modoki and its possible teleconnection. *J Geophys Res* 112:C11007
- Battisti DS, Hirst AG (1989) Interannual variability in a tropical atmosphere-ocean model: Influence of the basic state, ocean geometry and nonlinearly. *J Atmos Sci* 46:1687–1712
- Battisti DS (1988) Dynamics and thermodynamics of a warming event in a coupled tropical atmosphere-ocean model. *J Atmos Sci* 45:2889–2919
- Bjerknes J (1969) Atmospheric teleconnections from the equatorial pacific. *Mon Weather Rev* 97:163–172
- Chan JCL (2005) Interannual and interdecadal variations of tropical cyclone activity over the western North Pacific. *Meteor Atmos Phys* 89:143–152
- Chen SF, Song LY (2019) The leading interannual variability modes of winter surface air temperature over Southeast Asia. *Clim Dyn* 52:4715–4734
- Chen SF, Wu R (2018) Impacts of winter NPO on subsequent winter ENSO: sensitivity to the definition of NPO index. *Clim Dyn* 50:375–389

- Chen SF, Yu B, Chen W (2014) An analysis on the physical process of the influence of AO on ENSO. *Clim Dyn* 42:973–989
- Chen SF, Chen W, Yu B (2017) The influence of boreal spring Arctic Oscillation on the subsequent winter ENSO in CMIP5 models. *Clim Dyn* 48:2949–2965
- Chen SF, Yu B, Chen W, Wu R (2018a) A review of atmosphere-ocean forcings outside the tropical Pacific on the El Niño–Southern Oscillation occurrence. *Atmosphere* 9:439
- Chen W, Ding SY, Feng J, Chen SF, Xue X, Zhou Q (2018b) Progress in the study of impacts of different types of ENSO on the East Asian monsoon and their mechanisms. *Chin J Atmos Sci* 42:640–655
- Chen SF, Wu R, Chen W (2018c) A strengthened impact of November Arctic Oscillation on subsequent tropical Pacific sea surface temperature variation since the late-1970s. *Clim Dyn* 51:511–529
- Chen SF, Wu R, Chen W (2018d) Modulation of spring northern tropical Atlantic sea surface temperature on the El Niño–Southern Oscillation–East Asian summer monsoon connection. *Int J Climatol* 38:5020–5029
- Chen SF, Wu R, Chen W (2019) Projections of climate changes over mid-high latitudes of Eurasia during boreal spring: uncertainty due to internal variability. *Clim Dyn* 53:6309–6327
- Chiang JCH, Sobel AH (2002) Tropical tropospheric temperature variations caused by ENSO and their influence on the remote tropical climate. *J Clim* 15:2616–2631
- Chiang JCH, Vimont DJ (2004) Analogous Pacific and Atlantic meridional modes of tropical atmosphere–ocean variability. *J Clim* 17:4143–4158
- Christian JR, Arora VK, Boer GJ, Cury CL, Zahariev K, Denman KL, Flato GM, Lee WG, Merryfield WJ, Roulet NT, Scinocca JF (2010) The global carbon cycle in the CCCma earth system model CanESM1: preindustrial control simulation. *J Geophys Res* 115:G03014
- Dai A, Bloecker CE (2019) Impacts of internal variability on temperature and precipitation trends in large ensemble simulations by two climate models. *Clim Dyn* 52:289–306
- Deser C, Knutti R, Solomon S, Phillips AS (2012a) Communication of the role of natural variability in future North American climate. *Nat Clim Change* 2:775–779
- Deser C, Phillips AS, Bourdette V, Teng H (2012b) Uncertainty in climate change projections: the role of internal variability. *Clim Dyn* 38:527–546. <https://doi.org/10.1007/s00382-010-0977-x>
- Deser C, Phillips AS, Alexander MA, Smoliak BV (2014) Projecting North American climate over the next 50 years: uncertainty due to internal variability. *J Clim* 27:2271–2296
- Duchon CE (1979) Lanczos filtering in one and two dimensions. *J Appl Meteorol* 18:1016–1022. [https://doi.org/10.1175/1520-0450\(1979\)018,1016:LFI0AT.2.0.CO;2](https://doi.org/10.1175/1520-0450(1979)018,1016:LFI0AT.2.0.CO;2)
- Gill AE (1980) Some simple solutions for heat-induced tropical circulation. *Q J R Meteorol Soc* 106:447–462
- Graf HF, Zanchettin D (2012) Central Pacific El Niño, the “subtropical bridge”, and Eurasian climate. *J Geophys Res* 117:D01102
- Gray WM (1984) Atlantic seasonal hurricane frequency. Part I: El Niño and 30 mb quasi-biennial oscillation influences. *Mon Weather Rev* 112:1649–1668
- Ham YG, Kug JS (2015) Role of North Tropical Atlantic SST on the ENSO Simulated Using CMIP3 and CMIP5 models. *Clim Dyn* 45:3103–3117
- Ham YG, Kug JS, Park JY, Jin FF (2013) Sea Surface temperature in the North Tropical Atlantic as a Trigger for El Niño/Southern Oscillation events. *Nat Geosci* 6:112–116
- Huang RH, Zhang R, Yan B (2001) Dynamical effect of the zonal wind anomalies over the tropical western Pacific on ENSO cycles. *Sci China Ser D Earth Sci* 44:1089–1098
- Huang RH, Chen W, Yan BL, Zhang RH (2004) Recent advances in studies of the interaction between the east Asian winter and summer monsoons and ENSO cycle. *Adv Atmos Sci* 21:407–424
- Jin FF (1997) An equatorial ocean recharge paradigm for ENSO. Part I: conceptual model. *J Atmos Sci* 54:811–829
- Jin R, Wu ZW, Zhang P (2018) Tibetan Plateau capacitor effect during the summer preceding ENSO: from the Yellow River climate perspective. *Clim Dyn* 51(1):57–71
- Joshi MK, Ha KJ (2019) Fidelity of CMIP5-simulated teleconnection between Atlantic multidecadal oscillation and Indian summer monsoon rainfall. *Clim Dyn* 52:4157–4176
- Kalnay E, Kanamitsu M, Kistler R, Collins W, Deaven D, Gandin L, Iredell M, Saha S, White G, Woollen J (1996) The NCEP/NCAR 40-year reanalysis project. *Bull Am Meteor Soc* 77:437–471
- Kay JE, Deser C, Phillips A, Mai A, Hannay C, Strand G, Arblaster JM, Bates SC, Danabasoglu G, Edwards J, Holland M, Kushner P, Lamarque JF, Lawrence D, Lindsay K, Middleton A, Munoz E, Neale R, Oleson K, Polvani L (2015) The Community Earth System Model (CESM) large ensemble project: a community resource for studying climate change in the presence of internal climate variability. *Bull Am Meteor Soc* 96:1333–1349
- Kirchmeier-Young MC, Zwiers FW, Gillett NP (2017) Attribution of extreme events in Arctic sea ice extent. *J Clim* 30:553–571
- Kucharski F, Joshi MK (2017) Influence of tropical south Atlantic sea surface temperatures on the Indian summer monsoon in CMIP5 models. *Q J R Meteorol Soc* 143:1351–1363
- Lengaigne M, Guilyardi E, Boulanger JP, Menkes C, Delecluse P, Inness P, Cole J, Slingo J (2004) Triggering of El Niño by westerly wind events in a coupled general circulation model. *Clim Dyn* 23:601–620
- Linkin ME, Nigam S (2008) The north pacific oscillation–west Pacific teleconnection pattern: mature-phase structure and winter impacts. *J Clim* 21:1979–1997
- Luo JJ, Behera SK, Masumoto Y, Yamagata T (2011) Impact of global ocean surface warming on seasonal-to-interannual climate prediction. *J Clim* 24:1626–1646
- Luo JJ, Wang G, Dommenget D (2018) May common model biases reduce CMIP5’s ability to simulate the recent Pacific La Niña-like cooling? *Clim Dyn* 50:1335–1351
- McPhaden MJ (2002) El Niño and La Niña: causes and global consequences. In: MacCracken MC, Perry JS (eds) *Encyclopedia of global environmental change*, vol 1. Wiley, Chichester, pp 353–370
- Mo KC (2000) Relationships between low-frequency variability in the Southern Hemisphere and sea surface temperature anomalies. *J Clim* 13:3599–3610
- Nakamura T, Tachibana Y, Honda M, Yamane S (2006) Influence of the Northern Hemisphere annular mode on ENSO by modulating westerly wind bursts. *Geophys Res Lett* 33:L07709
- Nakamura T, Tachibana Y, Shimoda H (2007) Importance of cold and dry surges in substantiating the NAM and ENSO relationship. *Geophys Res Lett* 34:L22703
- Neelin JD, Battisti DS, Hirst AC, Jin FF, Wakata Y, Yamagata T, Zebiak SE (1998) ENSO theory. *J Geophys Res* 103:14261–14290
- Park JY, Yeh SW, Kug JS, Yoon J (2013) Favorable connections between seasonal footprinting mechanism and El Niño. *Clim Dyn* 40:1169–1181
- Pegion K, Alexander M (2013) The seasonal footprinting mechanism in CFSv2: simulation and impact on ENSO prediction. *Clim Dyn* 41:1671–1683
- Philander SG (1990) *El Niño, La Niña, and the Southern Oscillation*, vol 46. Academic Press, London
- Rong X, Zhang R, Li T (2010) Impacts of Atlantic sea surface temperature anomalies on Indo-East Asian summer monsoon–ENSO relationship. *Chin Sci Bull* 55:2458–2468
- Schopf PS, Suarez MJ (1988) Vacillations in a coupled ocean–atmosphere model. *J Atmos Sci* 45:549–566

- Sigmond M, Fyfe JC (2016) Tropical Pacific impacts on cooling North American winters. *Nat Clim Change* 6:970–974
- Smith TM, Reynolds RW, Peterson TC, Lawrimore J (2008) Improvements to NOAA's historical merged land-ocean surface temperature analysis (1880–2006). *J Clim* 21:2283–2296
- Song LY, Li Y, Duan W (2016) The influence of boreal winter extratropical North Pacific Oscillation on Australian spring rainfall. *Clim Dyn* 47:1181–1196
- Song LY, Chen SF, Chen W, Chen XL (2017) Distinct impacts of two types of La Niña events on Australian summer rainfall. *Int J Climatol* 37:2532–2544
- Vimont DJ, Battisti DS, Hirst AC (2001) Footprinting: a seasonal connection between the tropics and mid-latitudes. *Geophys Res Lett* 28:3923–3926
- Vimont DJ, Wallace JM, Battisti DS (2003a) The seasonal footprinting mechanism in the Pacific: implications for ENSO. *J Clim* 16:2668–2675
- Vimont DJ, Battisti DS, Hirst AC (2003b) The seasonal footprinting mechanism in the CSIRO general circulation models. *J Clim* 16:2653–2667
- Vuuren DP et al (2011) The representative concentration pathways: an overview. *Clim Change* 109:5–31
- Wallace JM, Gutzler DS (1981) Teleconnections in the geopotential height field during the northern hemisphere winter. *Mon Weather Rev* 109:784–812
- Wallace JM, Deser C, Smoliak BV, Phillips AS (2014) Attribution of climate change in the presence of internal variability. Climate change: multidecadal and beyond. In: Chang CP et al (eds) Asia-Pacific weather and climate series, vol 6. World Scientific, Singapore
- Wang B, Wu R, Fu X (2000) Pacific-East Asia teleconnection: How does ENSO affect East Asian climate? *J Clim* 13:1517–1536
- Wang X, Chen M, Wang C, Yeh S, Tan W (2019) Evaluation of performance of CMIP5 models in simulating the North Pacific oscillation and El Niño Modoki. *Clim Dyn* 52:1383–1394
- Wu R, Hu ZZ, Kirtman BP (2003) Evolution of ENSO-related rainfall anomalies in East Asia. *J Clim* 16:3742–3758
- Wu R, Kinter JL (2010) Atmosphere-ocean relationship in the midlatitude North Pacific: seasonal dependence and east-west contrast. *J Geophys Res* 115:D06101
- Xie SP, Hu K, Hafner J, Tokinaga H, Du Y, Huang G, Sampe T (2009) Indian ocean capacitor effect on Indo-Western Pacific climate during the summer following El Niño. *J Clim* 22:730–747
- Yu JY, Kim ST (2011) Relationships between extratropical sea level pressure variations and the central Pacific and eastern Pacific types of ENSO. *J Clim* 24:708–720
- Yu B, Zwiers F (2007) The impact of combined ENSO and PDO on the PNA climate: a 1000-year climate modeling study. *Clim Dyn* 29:837–851
- Yu JY, Lu MM, Kim ST (2012) A change in the relationship between tropical central Pacific SST variability and the extratropical atmosphere around 1990. *Environ Res Lett* 7:034025
- Zhang P, Wu ZW, Chen H (2017) Interdecadal VARIABILITY of the ENSO–North Pacific atmospheric circulation in winter. *Atmos Ocean* 55(2):110–120
- Zhang L, Xu H, Shi N, Ma J (2018) Impact of the North Pacific subtropical sea surface temperature front on El Niño–Southern Oscillation. *Int J Climatol* 38:e729–e740
- Zhang P, Wang B, Wu ZW (2019a) Weak El Niño and winter climate in the mid-to high latitudes of Eurasia. *J Clim* 32(2):405–421
- Zhang P, Wu ZW, Li JP (2019b) Reexamining the relationship of La Niña and the East Asian Winter Monsoon. *Clim Dyn*. <https://doi.org/10.1007/s00382-019-04613-7>
- Zhao W, Chen SF, Chen W, Yao SL, Nath D, Yu B (2019) Interannual variations of the rainy season withdrawal of the monsoon transitional zone in China. *Clim Dyn* 53:2031–2046
- Zheng XT, Hui C, Yeh SW (2018) Response of ENSO amplitude to global warming in CESM large ensemble: uncertainty due to internal variability. *Clim Dyn* 50:4019–4035. <https://doi.org/10.1007/s00382-017-3859-7>

Publisher's Note Springer Nature remains neutral with regard to jurisdictional claims in published maps and institutional affiliations.